0031-3998/08/6405-0488
PEDIATRIC RESEARCH

Vol. 64, No. 5, 2008
Printed in U.S.A.

A Mouse Model for Juvenile Doxorubicin-Induced Cardiac Dysfunction

WUQIANG ZHU, WEINIAN SHOU, R. MARK PAYNE, RANDALL CALDWELL, AND LOREN J. FIELD

Riley Heart Research Center, Wells Center for Pediatric Research [W.Z., W.S., R.M.P., R.C., L.J.F.], and the Krannert Institute of Cardiology [L.J.F.], Indiana University School of Medicine, Indianapolis, Indiana 26202

ABSTRACT: Doxorubicin (DOX) is a potent antitumor agent. DOX can also induce cardiotoxicity, and high cumulative doses are associated with recalcitrant heart failure. Children are particularly sensitive to DOX-induced heart failure. The ability to genetically modify mice makes them an ideal experimental system to study the molecular basis of DOX-induced cardiotoxicity. However, most mouse DOX studies rely on acute drug administration in adult animals, which typically are analyzed within 1 wk. Here, we describe a juvenile mouse model of chronic DOX-induced cardiac dysfunction. DOX treatment was initiated at 2 wk of age and continued for a period of 5 wk (25 mg/kg cumulative dose). This resulted in a decline in cardiac systolic function, which was accompanied by marked atrophy of the heart, low levels of cardiomyocyte apoptosis, and decreased growth velocity. Other animals were allowed to recover for 13 wk after the final DOX injection. Cardiac systolic function improved during this recovery period but remained depressed compared with the saline injected controls, despite the reversal of cardiac atrophy. Interestingly, increased levels of cardiomyocyte apoptosis and concomitant myocardial fibrosis were observed after DOX withdrawal. These data suggest that different mechanisms contribute to cardiac dysfunction during the treatment and recovery phases. (***Pediatr Res*** **64: 488–494, 2008)**

Etiologies of childhood cardiomyopathy are diverse, however, one of the most common is chemotherapy, such as anthracycline-induced cardiotoxicity (1). The anthracyclines, primarily doxorubicin (DOX) but also daunomycin, epirubicin, and idarubicin, are among the most widely used and successful chemotherapeutics for childhood cancers. About half of the young adult survivors of childhood cancer have received anthracyclines at some point in their treatment. Unfortunately, these drugs are also cardiotoxic. The acute responses to anthracyclines include hypotension, tachycardia, arrhythmia, and transient depression of left ventricular function (2–4). Higher cumulative doses are associated with late-onset cardiomyopathy that is refractory to standard treatment and thus limits the total amount of DOX, which may be administered (5,6). Children and adolescents are particularly susceptible to the cardiotoxic effects of anthracycline chemotherapy, and a significant portion of children treated with DOX develop cardiomyopathy a year or more after cessation of chemotherapy (5,7–9).

Although the precise mechanism underlying DOX-induced cardiotoxicity is uncertain (10,11), most studies indicate that free radical-induced oxidative stress plays a central role. Anthracyclines undergo one electron reduction by complex I in mitochondria (12) and in the process generate superoxide and hydroxyl radical (13). Reactive oxygen species-induced mitochondrial damage is thought to contribute to DOX-induced cardiotoxicity (14). DOX is also known to promote DNA damage and inhibit DNA and protein synthesis (15–17), promote myofiber degeneration (18), inhibit expression of cardiomyocyte specific genes (19), and induce cardiomyocyte apoptosis *via* a caspase 3-dependent mechanism (20–23). Thus, DOX-induced cardiotoxicity is complex and multifaceted.

Animal models have been widely used to study the molecular basis underlying DOX cardiotoxicity, and to develop strategies aimed at evoking therapeutic cardioprotection (24). Given the ease of generating specific gain- and loss-of-function genetic models, mice are particularly useful for DOX cardiotoxicity studies. Since children can be expected to survive for decades after being cured of their malignancy, albeit with a propensity for subsequently developing heart failure, an important component of any animal model should be persistent cardiac dysfunction after anthracycline withdrawal. Here, we describe a DOX-induced cardiotoxicity model using juvenile mice. DOX administration for 5 wk resulted in a decline in cardiac systolic function, which was accompanied by a marked atrophy of the cardiac muscle, low levels of cardiomyocyte apoptosis, and myofiber disarray. Reversal of cardiac atrophy and normalization of myofiber organization were observed after a 13-wk recovery period. Despite this, cardiac systolic function remained suppressed and was accompanied by an increased level of cardiomyocyte apoptosis and concomitant myocardial fibrosis. The implications and potential utility of this model are discussed.

METHODS

DOX treatment. Juvenile DBA/2J mice received a total of 25 mg/kg of DOX (5 intra-peritoneal injections of 5 mg/kg in saline, given at 7-d intervals beginning at 14 d of age, Sigma Chemical Co., St. Louis, MO; control mice received saline injections). To avoid local tissue damage, a different region of the peritoneal cavity was injected at each time point, and no overt inflammation/tissue damage was apparent. One cohort of mice was killed 1 wk after the final DOX injection to study acute cardiotoxicity (treatment phase). A second cohort was killed 13 wk after the final DOX injection to study the chronic

Received February 12, 2008; accepted June 20, 2008.
Correspondence: Loren Field, Ph.D., Wells Center, 1044 West Walnut Street, R4 Building Room W376, Indianapolis, IN 46202; e-mail: ljfield@iupui.edu
Supported by grants from the National Heart, Lung, and Blood Institute, National Institutes of Health.

Abbreviations: DOX, doxorubicin; **FS,** fractional shortening

effects of the drug (recovery phase). Mortality with this protocol was 10%. All animal protocols were approved by the Indiana University School of Medicine Institutional Animal Care and Use Committee.

Echocardiography. Transthoracic echocardiography was performed immediately before each DOX injection during the treatment phase, and then monthly during the recovery phase, as previously described (25). Mice were lightly anesthetized with 1.5% isofluorane until the heart rate stabilized at 400 to 500 beats per minute. Two-dimensional short-axis images were obtained using a high resolution Micro-Ultrasound system (Vevo 770, VisualSonics Inc., Toronto, Canada, 40-MHz probe). Left ventricular internal diameter during diastole, left ventricular internal diameter during systole, and fractional shortening (FS) were calculated using the Vevo Analysis software (version 2.2.3) as described (25).

Tissue and serum analyses. Tissues were harvested and processed for cryo or paraffin sectioning using standard techniques (26). Hematoxylin and Eosin staining was performed according to the manufacturer's protocols (Sigma Chemical Co. Diagnostics, St. Louis, MO). Minimal cardiomyocyte fiber diameter was calculated as described (27). At least 400 randomly selected cardiomyocytes from each animal were analyzed. Cardiac α-actinin (antibody EA-53, Sigma Chemical Co. Diagnostics, St. Louis, MO) immune reactivity was performed on permeiabilized, postfixed sections (rhodamine conjugated secondary antibody). Activated caspase-3 immune reactivity (antibody #G7481, Promega, Madison, WI) was performed on postfixed sections (horseradish peroxidase-conjugated secondary antibody, diaminobenzidine reaction) as described previously (28). Four transverse sections from each heart, sampled from the midpoint between the apex and base, were analyzed. TUNEL analyses were performed on adjacent sections using the ApopTag Apoptosis Detection kit according to the manufacturer's procedures (Chemicon International, Billerica, MA). Sirius red-Fast green staining was performed and quantitated on sections postfixed in Bouin's solution as described previously (29,30). Hematocrit and hematologic analyses were performed using standard analyses. Serum Troponin I levels were determined using a commercial ELISA kit (Life Diagnostics, Inc., West Chester, PA).

Western blot analyses. Protein was isolated in NP40 buffer and subjected to Western analysis as previously described (31,32). Antibodies used recognized myosin heavy chain (H-300, #SC-20641, Santa Cruz Biotechnologies, Santa Cruz, CA), phosphorylated GSK3β (#9331, Cell Signaling Technology, Danvers, MA), total GSK3β, (#9315, Cell Signaling Technology), phosphorylated Akt (#9271, Cell Signaling Technology) and total Akt (#9272, Cell Signaling Technology). Signal was visualized by the ECL method according to the manufacturer's protocol (Amersham).

Statistic analysis. All values are presented as mean $\pm$ SEM. Statistical significance ($p < 0.01$) was determined by t test (for groups of two), or by one-way ANOVA with Bonferroni adjustment (for groups of three or more).

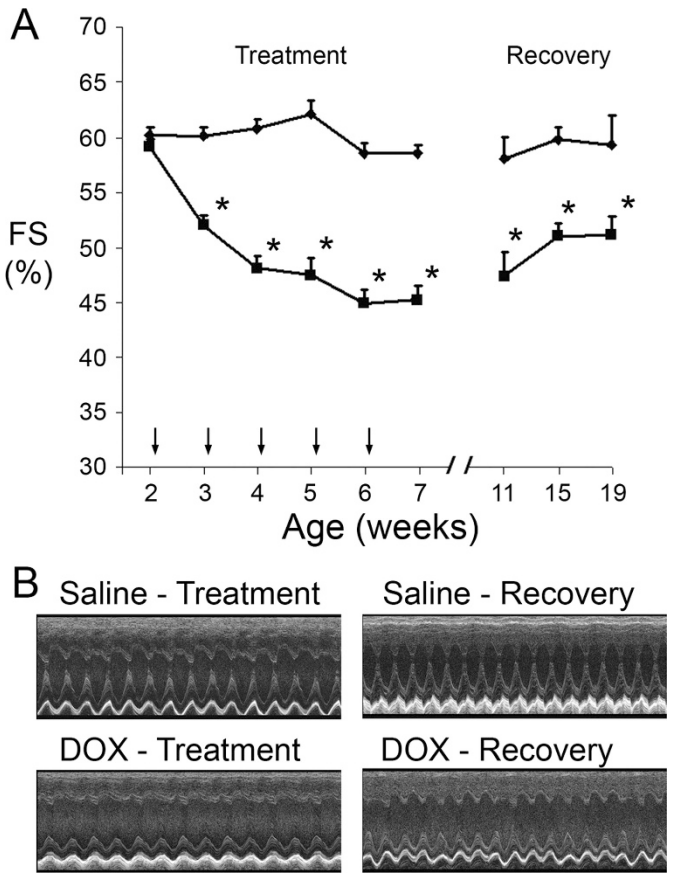

Figure 1. Cardiac function in saline- and DOX-injected juvenile mice. (*A*) Fractional Shortening (FS [%]) in saline-injected (*diamonds*) and DOX-injected (*squares*) mice during the treatment and recovery phases. X-axis indicates the age of the mice at analysis; vertical arrows indicate the age of injection. "*" indicates $p < 0.01$ for DOX-injected *vs.* saline-injected mice. (*B*) Representative short axis echocardiograms from saline- and DOX-injected mice at the end of the treatment and recovery phases.

RESULTS

Juvenile DBA/2J mice received weekly injections of saline or DOX, beginning at 2 wk of age and continuing for a period of 5 wk. Echocardiography was used to measure FS of the short axis of the left ventricle. Baseline FS was similar before the initiation of saline or DOX treatment (Fig. 1*A*, Table 1). Cardiac function in the saline-injected mice remained constant over the 5-wk treatment phase with an FS of approximately 60%. In contrast, FS was suppressed 1 wk after the first DOX-injection, and remained suppressed with a value of approximately 45% at the end of the treatment phase (Fig. 1*A*, Table 1). These animals were killed for cell and molecular analyses (see below). Importantly, DOX-treatment had the anticipated impact on hematologic parameters, and serum cardiac Troponin I ELISA analyses indicated the presence of myocardial damage (Table 2).

A second group of mice subjected to the same regimen of saline or DOX injection was allowed to recover for 13 wk. DOX treatment resulted in a similar decrease in cardiac function (not shown). Cardiac function remained suppressed in the DOX-injected animals throughout the entire recovery phase compared with the saline-injected controls (Fig. 1*A*). Decreased left ventricular contraction was apparent in representative echocardiograms from DOX-injected mice at the end of the treatment and recovery phases, compared with the saline-injected controls (Fig. 1*B*). Of interest, mechanical alternans were occasionally observed in the DOX-injected group.

Growth velocity was markedly lower in the DOX-injected animals during the treatment phase compared with the saline-injected mice. Although growth velocity was similar in the two groups during the recovery phase, absolute body weight was less in the DOX treated animals due to growth inhibition during the treatment phase (Fig. 2*A*). A reduction in heart weight was noted at the end of the treatment phase in DOX-injected animals compared with saline-injected control animals. However, by the end of the recovery phase heart weight in DOX-injected mice was largely restored, approaching values observed in control animals (Fig. 2*B*). A similar result was obtained when heart weight was normalized to tibia length (Fig. 2*C*).

Hearts harvested at the end of the treatment and recovery phases were processed for histochemical analysis. Survey micrographs from Hematoxylin and Eosin (H&E) stained sections suggested a reduction in left ventricular wall thickness in DOX-injected animals at the end of the treatment phase, which appeared to return to normal by the end of the

Table 1. *Cardiac function in saline- and DOX-injected juvenile mice (Mean ± SEM)*

Age (weeks)	2	3	4	5	6	7	11	15	19
	n = 10						n = 11		
Saline									
HR (bpm)	451 ± 9	452 ± 12	458 ± 10	494 ± 14	479 ± 12	473 ± 11	480 ± 13	470 ± 8	468 ± 13
LVIDD (mm)	2.2 ± 0.1	2.4 ± 0.1	2.6 ± 0.1	2.6 ± 0.1	2.6 ± 0.1	2.7 ± 0.10	2.7 ± 0.1	2.8 ± 0.2	2.9 ± 0.3
LVIDS (mm)	0.9 ± 0.0	1.0 ± 0.1	1.0 ± 0.0	1.0 ± 0.0	1.1 ± 0.0	1.1 ± 0.0	1.1 ± 0.0	1.1 ± 0.0	1.2 ± 0.1
FS (%)	60 ± 0.7	60 ± 0.7	61 ± 0.9	62 ± 1.2	59 ± 0.9	59 ± 0.7	58 ± 1.9	60 ± 1.2	59 ± 2.6
	n = 11						n = 17		
DOX									
HR (bpm)	426 ± 8	445 ± 14	426 ± 14	454 ± 11	444 ± 7	469 ± 13	452 ± 15	476 ± 13	478 ± 11
LVIDD (mm)	2.2 ± 0.1	2.6 ± 0.1	2.6 ± 0.1	2.8 ± 0.1	2.6 ± 0.1	2.8 ± 0.1	2.7 ± 0.1	2.9 ± 0.1	2.9 ± 0.1
LVIDS (mm)	0.9 ± 0.0	1.2 ± 0.0*	1.4 ± 0.1*	1.5 ± 0.1*	1.4 ± 0.0*	1.5 ± 0.1*	1.4 ± 0.1*	1.4 ± 0.1*	1.4 ± 0.1
FS (%)	59 ± 0.7	52 ± 0.9*	48 ± 1.1*	47 ± 1.5*	45 ± 1.3*	45 ± 1.3*	47 ± 2.2*	51 ± 1.2*	51 ± 1.8*

* $p < 0.05$ vs. Saline-treated mice.

Table 2. *Blood cell counts and cTnI concentration measurements (Mean ± SEM)*

Leukocytes	WBC (K/uL)	NE (K/uL)	LY (K/uL)	MO (K/uL)	EO (K/uL)	BA (K/uL)	
Saline (n = 12)	12.71 ± 1.27	4.08 ± 0.48	7.23 ± 0.79	0.59 ± 0.10	0.65 ± 0.24	0.16 ± 0.05	
DOX (n = 16)	6.92 ± 0.96*	4.13 ± 0.72	2.04 ± 0.21*	0.41 ± 0.10	0.27 ± 0.09	0.08 ± 0.03	
Erythrocytes	RBC (M/uL)	HB (g/dL)	HCT (%)	MCV (fL)	MCH (pg)	MCHC (g/dL)	RDW (%)
Saline (n = 12)	10.08 ± 0.26	13.51 ± 0.33	51.96 ± 1.25	51.62 ± 0.57	13.42 ± 0.11	26.02 ± 0.29	22.57 ± 0.28
DOX (n = 16)	7.30 ± 0.65*	9.79 ± 0.92*	39.45 ± 3.61*	53.54 ± 0.68*	13.22 ± 0.24	24.66 ± 0.24*	24.62 ± 0.56*
cTnI	ng/mL						
Saline (n = 12)	0.31 ± 0.20						
DOX (n = 16)	4.56 ± 1.19*						

WBC, white blood cells; NE, neutrophils; LY, lymphocytes; MO, monocytes; EO, eosiniohils; BA, basophils; K/uL, 1000 cells per microliter; RBC, red blood cells; HB, hemoglobin; HCT, hematocrit; MCV, mean corpuscular volume; MCH, mean corpuscular hemaglobin; MCHC, mean corpuscular hemoglobin content; RDW, red blood cell distribution width. * $p < 0.05$ vs. Saline-treated mice.

recovery period (Fig. 2*D*). Quantitative morphometric analyses were performed to validate these gross observations. Previous studies have shown that minimal fiber diameter (MFD) measurements can be used as an index for cardiomyocyte hypertrophy or atrophy in histology sections (33). A reduction in cardiomyocyte MFD was observed at the end of the treatment phase in hearts from DOX-injected mice (Fig. 2*E*). This suggests that the DOX-induced decrease in heart weight resulted at least in part from cardiomyocyte atrophy. Interestingly, cardiomyocyte MFD in hearts from DOX-injected mice returned to control values during the recovery phase.

Anti-cardiac α-actinin immune reactivity was monitored to ascertain the impact of DOX on myofiber structure (Fig. 3*A*). Well organized sarcomeric structure was apparent in hearts from saline-injected animals during the treatment and recovery phases. In contrast, myofiber structure was disrupted in hearts from DOX-injected animals during the treatment phase, as evidenced by the widespread reduction of sarcomeric staining. Sarcomeric structure was reorganized by the end of the recovery phase in hearts from DOX-injected animals.

Anti-activated caspase 3 immune histology was used to quantitate cardiomyocyte apoptosis in hearts from saline- and DOX-injected mice. Since activated caspase 3 is distributed in the cytoplasm, cardiomyocytes at early stages of apoptosis were easily identified by the presence of immune reactivity in rod-shaped cells (28). Figure 4*A* shows a representative image of an activated caspase 3 immune reactive cardiomyocyte from a DOX-treated heart. An approximately 5-fold increase in the number of activated caspase 3 immune reactive cardiomyocytes per mm^2 myocardium was observed in DOX-injected mice at the end of the treatment phase compared with saline-injected controls (Fig. 4*B*). Interestingly, the level of cardiomyocyte apoptosis was higher in the DOX treated animals at the end of the recovery phase (*i.e.* 13 wk after the last drug injection, see Fig. 4*B*). A similar increase in the number of apoptotic cells was obtained using TUNEL staining as an index for apoptosis, with a 4.5 ± 0.3-fold increase in DOX-injected mice at the end of the treatment phase ($n = 5$), and a 19.5 ± 2.5-fold increase at the end of the recovery phase ($n = 6$), compared with the respective saline-injected controls ($n = 7$).

Sirius red-Fast green-staining was performed to monitor the level of myocardial collagen deposition, which is indicative of fibrosis. Representative images shown in Fig. 5*A* indicate that collagen deposition (red signal) was minimal at the end of the treatment phase in hearts from DOX-injected mice, but become prevalent at the end of the recovery phase. Quantitative image analyses confirmed this observation, consistent with the presence of DOX-induced myocardial fibrosis (Fig. 5*B*). Finally, Western blot analyses were performed to monitor the expression and/or activity of several myocardial proteins, which are known to be modulated by DOX (Fig. 6). Lower levels of myosin heavy chain, phosphorylated glycogen synthase kinase (GSK)3β, and phosphorylated Akt were apparent in hearts from DOX-injected animals at the end of the treatment phase, compared with the saline-injected controls. DOX treatment had no effect on total GSK3β or Akt levels. At the end of the recovery phase, expression of these proteins in hearts from DOX-injected mice returned those seen in the saline-injected animals.

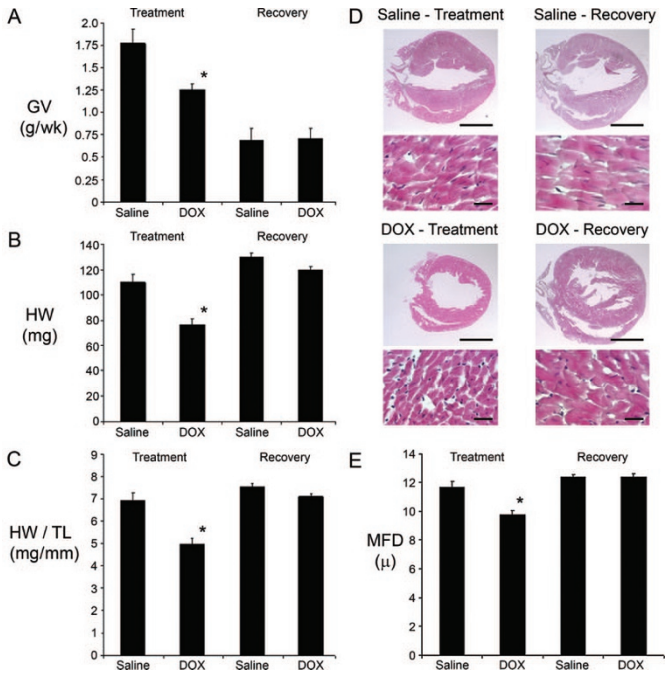

Figure 2. Growth parameters and histochemical analysis of saline- and DOX-injected juvenile mice. (*A*) Growth velocity (GV [g/wk]) during the treatment and recovery phases. (*B*) Heart weight in milligrams (HW [mg]) at the end of the treatment and recovery phases. (*C*) Heart weight/tibia length (HW/TL) measurements at the end of the treatment and recovery phases. (*D*) Representative survey and high power micrographs of heart sections from mice at the end of the treatment and recovery phases. Note the thin left ventricular wall in the heart from the DOX-injected mouse at the end of the treatment phase. Magnification bar in the survey micrographs = 2 mm; magnification bar in the high power micrographs = 20 μm. (*E*) Cardiomyocyte MFD measurements at the end of the treatment and recovery phases. For all panels, "*" indicates $p < 0.01$ for DOX-injected *vs.* saline-injected mice.

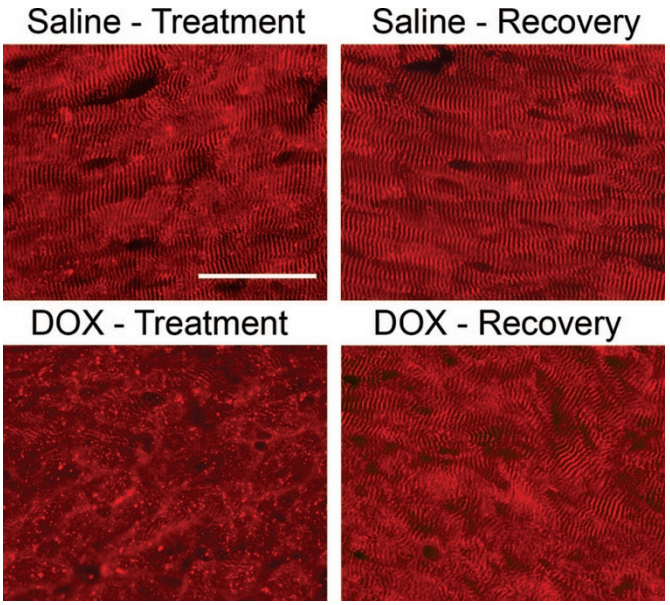

Figure 3. Myocardial alterations induced by DOX treatment. Cardiac α-actinin immune reactivity in hearts from saline- and DOX-injected mice during the treatment and recovery phases (rhodamine-conjugated secondary antibody, red signal). Magnification bar = 50 μm.

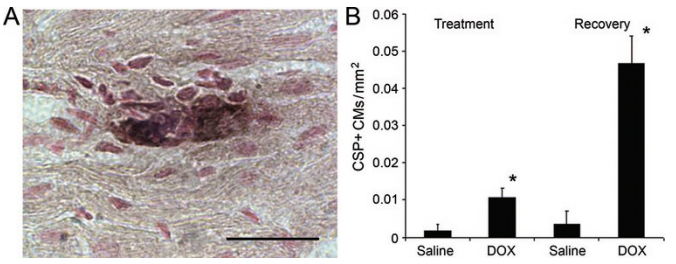

Figure 4. Cardiomyocyte activated caspase 3 immune reactivity in saline- and DOX-injected juvenile mice. (*A*) Representative image of an anti-activated caspase 3 immune-reactive cardiomyocyte from a DOX-injected heart harvested at the end of the treatment phase. Magnification bar = 20 μm. (*B*) Number of activated caspase 3 immune-reactive cardiomyocytes (CSP+) per mm^2 at the end of the treatment and recovery phases. *Indicates $p < 0.01$ for DOX-injected *vs.* saline-injected mice.

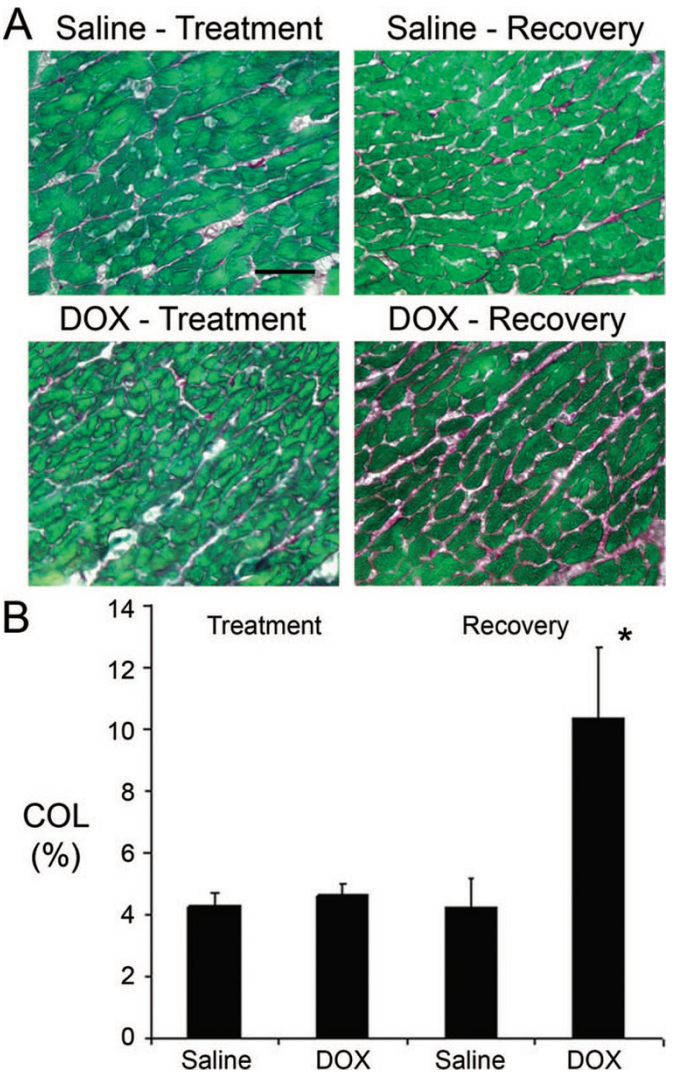

Figure 5. Myocardial fibrosis in saline- and DOX-injected juvenile mice. (*A*) Representative images of Sirius red-Fast green stained sections from hearts harvested at the end of the treatment and recovery phases. Red signal indicates collagen deposition. Magnification bar = 40 μm. (*B*) Collagen (COL) content at the end of the treatment and recovery phases. "*" Indicates $p < 0.01$ for DOX-injected *vs.* saline-injected mice.

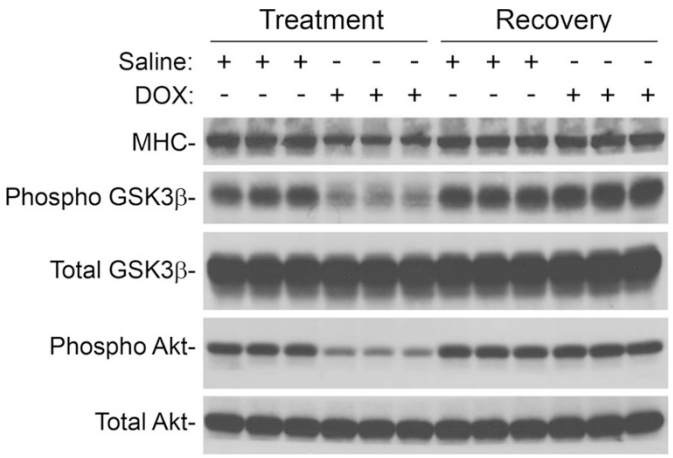

Figure 6. Western blot analysis of protein expression in hearts from saline- and DOX-injected mice during the treatment and recovery phases. Equal protein loading between samples was confirmed by Napthol blue staining of the membrane before hybridization (not shown).

DISCUSSION

The results presented here demonstrate that treatment of juvenile mice with DOX resulted in cardiotoxicity manifested by decreased cardiac systolic function, as well as heart and cardiomyocyte atrophy, myofiber disarray, low levels of cardiomyocyte apoptosis, and altered expression of structural and regulatory proteins. Cardiac systolic dysfunction persisted for as long as 13 wk after the termination of DOX treatment (the latest time-point analyzed) despite the normalization of organ mass, cell mass, myofiber structure, and protein expression. Cardiac dysfunction in the recovery phase was accompanied by increased levels of cardiomyocyte apoptosis and myocardial fibrosis.

In the vast majority of mouse DOX cardiotoxicity studies, animals typically received a single injection of drug and were analyzed within 1 wk. None used juvenile mice. Nonetheless, several published studies share methodological aspects with the current work, and as such provide an interesting comparison. For example, adult mice receiving cumulative DOX doses of 15 mg/kg (34,35) to 24 mg/kg (36) and analyzed at 2 (34), 4 (36), or 8 (35) weeks after the last drug injection all exhibited sustained depression of cardiac function. Somewhat surprisingly, the two studies using a 15 mg/kg cumulative DOX dose differed markedly with respect to the level of cardiomyocyte apoptosis, with no apoptosis detected at 2 wk post drug delivery in one study (34) and consistently elevated levels of apoptosis at 0, 2, 4, and 8 wk after the last drug injection in the other study (35). In contrast, the levels of cardiomyocyte apoptosis observed in our study were more dynamic. Difficulties encountered when identifying cardiomyocyte nuclei in histology sections (37) may explain the discrepant levels of apoptosis reported in the previous studies, as the TUNEL and *in situ* end labeling (ISEL) analyses used label both cardiomyocyte and nonmyocyte nuclei. The use of activated caspase 3 immune reactivity in the current study (which permitted cardiomyocyte identification *via* morphologic criteria) circumvented this problem.

Although it is well known that acute DOX cardiotoxicity is associated with myofiber disarray and cardiomyocyte shrinkage (38), the marked reduction in heart weight and cardiomyocyte size observed at the end of the treatment period was somewhat unexpected. Several recent studies observed a similar impact on heart weight and/or cardiomyocyte MFD (39–42) after a single injection of DOX (15 mg/kg) in adult mice. Myofiber disarray was also apparent in adult mice receiving a single or multiple injections of DOX (12–15 mg/kg cumulative dose) for as long as 2 wk after drug delivery (39,41,43). Myofiber disarray appears to result at least in part from calpain-induced degradation of titin (18). Similar to our results, Yoda and colleagues observed reversal of myofiber disarray 56 d after a single injection of DOX at 14 mg/kg (44).

Several studies have described DOX-induced changes in protein expression similar to that observed in the current study (19,38,39,45). This occurs at least in part *via* phosphoregulation of both ubiquitous and cardiac-restricted transcriptional co-factors (46,47). In addition, recent studies using a reporter transgene, which targets cardiac-restricted expression of enhanced green fluorescent protein engineered to carry ubiquination signal sequence demonstrated that DOX treatment results in a marked induction of 26-proteosome activity (48). Collectively, these transcriptional and proteolytic processes likely contribute to the cardiomyocyte atrophy and myofiber disarray observed during the treatment phase of the current study.

Different mechanisms may contribute to the cardiac systolic dysfunction observed in the treatment *versus* recovery phases in the model presented here. Cardiomyocyte atrophy, loss of myofiber sarcomeric structure, and altered protein expression are likely major contributors to cardiac dysfunction during the DOX treatment phase. Given the relatively low levels of cardiomyocyte apoptosis and the absence of reactive fibrosis, these processes may have little or no impact on cardiac function during the treatment phase of the model. Although the decreased growth velocity and cardiac systolic function observed in the DOX-treated animals, as well as the absence of overt histopathology in the kidney and gut (not shown), is consistent with the presence of heart failure, the lack of standardized definition for heart failure in mice makes it somewhat tenuous to apply this designation. Unfortunately, many of the ancillary analyses, which would assist in diagnosing heart failure, cannot be performed on mice at the ages studied during the treatment phase.

In contrast, the DOX-induced changes in cardiomyocyte size, myofiber organization and protein expression returned to control values during the recovery phase, and thus are likely not to have contributed to the sustained cardiac dysfunction. Rather, a marked increase in cardiomyocyte apoptosis and concomitant induction myocardial fibrosis was observed. Increased extracellular matrix content contributes to diastolic stiffness, and ultimately promotes ventricular dysfunction (49). Thus, apoptosis-induced fibrosis may be a major contributor to the depressed cardiac function observed during the recovery phase in this model.

Although a similar mechanism may underlie the appearance of heart failure in children previously treated with DOX, it is important to acknowledge the limitations of the current study. Notably, a decrease in left ventricular wall thickness is observed in the long-term survivors of anthracycline therapy in childhood. In contrast, wall thickness appeared to have normalized during the recovery phase in the mouse model. However, given the presence of sustained cardiomyocyte apoptosis and concomitant myocardial fibrosis at the end of the recovery phase, wall thinning and frank heart failure may very well occur at later time points. Another potential concern is that the limited blood volume in mice precluded clinical chemistry analysis, which would have been helpful to determine the extent to which noncardiac tissue damage may have contributed to myocardial dysfunction. However, this caveat could be unequivocally addressed by experiments employing mice harboring cardiac-restricted, cardioprotective genetic modifications.

In light of the multifaceted nature of DOX-induced cardiotoxicity (see Introduction), other mechanisms are also likely to contribute to the phenotypes observed during the treatment and recovery phases. Nonetheless, if the interpretation of our data is correct, studies examining cardioprotective interventions in models utilizing a single injection of DOX followed by a short recovery period might benefit from re-evaluation. In particular, reassessment of therapeutics aimed at inducing cardioprotection by blocking apoptosis during acute DOX cardiotoxicity is likely to be warranted (11). Evaluation of genetically modified mice using the DOX-induced model described here could help address this important issue.

Acknowledgments. The authors thank Dorothy Field for excellent technical assistance, and Drs. Michael Rubart, Mark Soonpaa and Alex Becker for comments on the manuscript.

REFERENCES

1. Morrow WR 2000 Cardiomyopathy and heart transplantation in children. Curr Opin Cardiol 15:216–223
2. Bristow MR, Billingham ME, Mason JW, Daniels JR 1978 Clinical spectrum of anthracycline antibiotic cardiotoxicity. Cancer Treat Rep 62:873–879
3. Lefrak EA, Pitha J, Rosenheim S, Gottlieb JA 1973 A clinicopathologic analysis of adriamycin cardiotoxicity. Cancer 32:302–314
4. Rinehart JJ, Lewis RP, Balcerzak SP 1974 Adriamycin cardiotoxicity in man. Ann Intern Med 81:475–478
5. Sorensen K, Levitt GA, Bull C, Dorup I, Sullivan ID 2003 Late anthracycline cardiotoxicity after childhood cancer: a prospective longitudinal study. Cancer 97:1991–1998
6. Singal PK, Iliskovic N 1998 Doxorubicin-induced cardiomyopathy. N Engl J Med 339:900–905
7. Lipshultz SE, Lipsitz SR, Sallan SE, Dalton VM, Mone SM, Gelber RD, Colan SD 2005 Chronic progressive cardiac dysfunction years after doxorubicin therapy for childhood acute lymphoblastic leukemia. J Clin Oncol 23:2629–2636
8. Steinherz LJ, Steinherz PG, Tan C 1995 Cardiac failure and dysrhythmias 6–19 years after anthracycline therapy: a series of 15 patients. Med Pediatr Oncol 24:352–361
9. Lipshultz SE, Colan SD, Gelber RD, Perez-Atayde AR, Sallan SE, Sanders SP 1991 Late cardiac effects of doxorubicin therapy for acute lymphoblastic leukemia in childhood. N Engl J Med 324:808–815
10. Singal PK, Li T, Kumar D, Danelisen I, Iliskovic N 2000 Adriamycin-induced heart failure: mechanism and modulation. Mol Cell Biochem 207:77–86
11. Takemura G, Fujiwara H 2007 Doxorubicin-induced cardiomyopathy from the cardiotoxic mechanisms to management. Prog Cardiovasc Dis 49:330–352
12. Davies KJ, Doroshow JH 1986 Redox cycling of anthracyclines by cardiac mitochondria. I. Anthracycline radical formation by NADH dehydrogenase. J Biol Chem 261:3060–3067
13. Doroshow JH, Davies KJ 1986 Redox cycling of anthracyclines by cardiac mitochondria. II. Formation of superoxide anion, hydrogen peroxide, and hydroxyl radical. J Biol Chem 261:3068–3074
14. Zhou S, Starkov A, Froberg MK, Leino RL, Wallace KB 2001 Cumulative and irreversible cardiac mitochondrial dysfunction induced by doxorubicin. Cancer Res 61:771–777
15. Arena E, D'Alessandro N, Dusonchet L, Geraci M, Rausa L, Sanguedolce R 1979 Repair kinetics of DNA, RNA and proteins in the tissues of mice treated with doxorubicin. Arzneimittelforschung 29:901–902
16. Billingham ME, Mason JW, Bristow MR, Daniels JR 1978 Anthracycline cardiomyopathy monitored by morphologic changes. Cancer Treat Rep 62:865–872
17. Monti E, Prosperi E, Supino R, Bottiroli G 1995 Free radical-dependent DNA lesions are involved in the delayed cardiotoxicity induced by adriamycin in the rat. Anticancer Res 15:193–197
18. Lim CC, Zuppinger C, Guo X, Kuster GM, Helmes M, Eppenberger HM, Suter TM, Liao R, Sawyer DB 2004 Anthracyclines induce calpain-dependent titin proteolysis and necrosis in cardiomyocytes. J Biol Chem 279:8290–8299
19. Papoian T, Lewis W 1991 Selective alterations in rat cardiac mRNA induced by doxorubicin: possible subcellular mechanisms. Exp Mol Pathol 54:112–121
20. Wang L, Ma W, Markovich R, Chen JW, Wang PH 1998 Regulation of cardiomyocyte apoptotic signaling by insulin-like growth factor I. Circ Res 83:516–522
21. Kitta K, Day RM, Kim Y, Torregroza I, Evans T, Suzuki YJ 2003 Hepatocyte growth factor induces GATA-4 phosphorylation and cell survival in cardiac muscle cells. J Biol Chem 278:4705–4712
22. Kim R, Tanabe K, Uchida Y, Emi M, Inoue H, Toge T 2002 Current status of the molecular mechanisms of anticancer drug-induced apoptosis. The contribution of molecular-level analysis to cancer chemotherapy. Cancer Chemother Pharmacol 50:343–352
23. Ueno M, Kakinuma Y, Yuhki K, Murakoshi N, Iemitsu M, Miyauchi T, Yamaguchi I 2006 Doxorubicin induces apoptosis by activation of caspase-3 in cultured cardiomyocytes in vitro and rat cardiac ventricles in vivo. J Pharmacol Sci 101:151–158
24. Herman EH, Ferrans VJ 1998 Preclinical animal models of cardiac protection from anthracycline-induced cardiotoxicity. Semin Oncol 25:15–21
25. Chen H, Yong W, Ren S, Shen W, He Y, Cox KA, Zhu W, Li W, Soonpaa M, Payne RM, Franco D, Field LJ, Rosen V, Wang Y, Shou W 2006 Overexpression of bone morphogenetic protein 10 in myocardium disrupts cardiac postnatal hypertrophic growth. J Biol Chem 281:27481–27491
26. Bullock GR, Petrusz P 1982 Techniques in Immunocytochemistry. London, New York: Academic Press
27. Soonpaa MH, Field LJ 1997 Assessment of cardiomyocyte DNA synthesis in normal and injured adult mouse hearts. Am J Physiol 272:H220–H226
28. Nakajima H, Nakajima HO, Tsai SC, Field LJ 2004 Expression of mutant p193 and p53 permits cardiomyocyte cell cycle reentry after myocardial infarction in transgenic mice. Circ Res 94:1606–1614
29. Nakajima H, Nakajima HO, Dembowsky K, Pasumarthi KB, Field LJ 2006 Cardiomyocyte cell cycle activation ameliorates fibrosis in the atrium. Circ Res 98:141–148
30. Pasumarthi KB, Nakajima H, Nakajima HO, Soonpaa MH, Field LJ 2005 Targeted expression of cyclin D2 results in cardiomyocyte DNA synthesis and infarct regression in transgenic mice. Circ Res 96:110–118
31. Towbin H, Staehelin T, Gordon J 1979 Electrophoretic transfer of proteins from polyacrylamide gels to nitrocellulose sheets: procedure and some applications. Proc Natl Acad Sci USA 76:4350–4354
32. Laemmli UK 1970 Cleavage of structural proteins during the assembly of the head of bacteriophage T4. Nature 227:680–685
33. Dubowitz V, Sewry CA, Fitzsimons RB 1985 Muscle biopsy: a practical approach. London; Philadelphia: Baillière Tindall, p 120
34. Kim KH, Oudit GY, Backx PH 2008 Erythropoietin protects against doxorubicin-induced cardiomyopathy via a phosphatidylinositol 3-kinase-dependent pathway. J Pharmacol Exp Ther 324:160–169
35. Fisher PW, Salloum F, Das A, Hyder H, Kukreja RC 2005 Phosphodiesterase-5 inhibition with sildenafil attenuates cardiomyocyte apoptosis and left ventricular dysfunction in a chronic model of doxorubicin cardiotoxicity. Circulation 111:1601–1610
36. Delgado RM III, Nawar MA, Zewail AM, Kar B, Vaughn WK, Wu KK, Aleksic N, Sivasubramanian N, McKay K, Mann DL, Willerson JT 2004 Cyclooxygenase-2 inhibitor treatment improves left ventricular function and mortality in a murine model of doxorubicin-induced heart failure. Circulation 109:1428–1433
37. Soonpaa MH, Field LJ 1998 Survey of studies examining mammalian cardiomyocyte DNA synthesis. Circ Res 83:15–26
38. Singal PK, Deally CM, Weinberg LE 1987 Subcellular effects of adriamycin in the heart: a concise review. J Mol Cell Cardiol 19:817–828
39. Esaki M, Takemura G, Kosai K, Takahashi T, Miyata S, Li L, Goto K, Maruyama R, Okada H, Kanamori H, Ogino A, Ushikoshi H, Minatoguchi S, Fujiwara T, Fujiwara H 2008 Treatment with an adenoviral vector encoding hepatocyte growth factor mitigates established cardiac dysfunction in doxorubicin-induced cardiomyopathy. Am J Physiol Heart Circ Physiol 294:H1048–H1057
40. Li K, Sung RY, Huang WZ, Yang M, Pong NH, Lee SM, Chan WY, Zhao H, To MY, Fok TF, Li CK, Wong YO, Ng PC 2006 Thrombopoietin protects against in vitro and in vivo cardiotoxicity induced by doxorubicin. Circulation 113:2211–2220
41. Li L, Takemura G, Li Y, Miyata S, Esaki M, Okada H, Kanamori H, Khai NC, Maruyama R, Ogino A, Minatoguchi S, Fujiwara T, Fujiwara H 2006 Preventive

effect of erythropoietin on cardiac dysfunction in doxorubicin-induced cardiomyopathy. Circulation 113:535–543
42. Li L, Takemura G, Li Y, Miyata S, Esaki M, Okada H, Kanamori H, Ogino A, Maruyama R, Nakagawa M, Minatoguchi S, Fujiwara T, Fujiwara H 2007 Granulocyte colony-stimulating factor improves left ventricular function of doxorubicin-induced cardiomyopathy. Lab Invest 87:440–455
43. Alderton PM, Gross J, Green MD 1992 Comparative study of doxorubicin, mitoxantrone, and epirubicin in combination with ICRF-187 (ADR-529) in a chronic cardiotoxicity animal model. Cancer Res 52:194–201
44. Yoda Y, Nakazawa M, Abe T, Kawakami Z 1986 Prevention of doxorubicin myocardial toxicity in mice by reduced glutathione. Cancer Res 46:2551–2556
45. Negoro S, Oh H, Tone E, Kunisada K, Fujio Y, Walsh K, Kishimoto T, Yamauchi-Takihara K 2001 Glycoprotein 130 regulates cardiac myocyte survival in doxorubicin-induced apoptosis through phosphatidylinositol 3-kinase/Akt phosphorylation and Bcl-xL/caspase-3 interaction. Circulation 103:555–561
46. Jeyaseelan R, Poizat C, Baker RK, Abdishoo S, Isterabadi LB, Lyons GE, Kedes L 1997 A novel cardiac-restricted target for doxorubicin. CARP, a nuclear modulator of gene expression in cardiac progenitor cells and cardiomyocytes. J Biol Chem 272:22800–22808
47. Poizat C, Puri PL, Bai Y, Kedes L 2005 Phosphorylation-dependent degradation of p300 by doxorubicin-activated p38 mitogen-activated protein kinase in cardiac cells. Mol Cell Biol 25:2673–2687
48. Kumarapeli AR, Horak KM, Glasford JW, Li J, Chen Q, Liu J, Zheng H, Wang X 2005 A novel transgenic mouse model reveals deregulation of the ubiquitin-proteasome system in the heart by doxorubicin. FASEB J 19:2051–2053
49. Swynghedauw B 1999 Molecular mechanisms of myocardial remodeling. Physiol Rev 79:215–262